

Novel surfactant-free multi-branched gold stars characterized by inverse photocurrent†

Cite this: DOI: 10.1039/c3ta11983a

Kang Yeol Lee,^a Minsik Kim,^b Jin-Seo Noh,^c Hee Cheul Choi^d and Wooyoung Lee^{*a}

Multi-branched gold stars were spontaneously formed on a semiconductor (Ge) substrate in high yield via a surfactant-free galvanic displacement method at room temperature using a DMF–water (9/1) mixed solvent. The average length of the branches was estimated to be 561 nm, and the size and shape of the multi-branched gold stars can be controlled by varying the reaction time of the Ge wafer and gold precursor. A high volume ratio of DMF was found to be crucial for the formation of these multi-branched gold stars. Interestingly, the photocurrent of the prepared gold stars decreased by 10% upon irradiation with a 532 nm visible laser. The photocurrent was switched on and off >10 times without significant degradation, indicating high reproducibility and reliability of the inverse photoresponse of the gold stars under visible light.

Received 20th May 2013

Accepted 11th September 2013

DOI: 10.1039/c3ta11983a

www.rsc.org/MaterialsA

Introduction

The unique plasmonic properties and electrical conductivity of metallic gold (Au) nanostructures have been of great interest due to their applications in catalysis, photonics, and biotechnology (biosensors, delivery and therapeutic applications).^{1–9} In particular, geometrically diverse Au nanostructures have been synthesized for various applications, including nanorods,¹⁰ multipods,¹¹ polyhedral particles,¹² and multi-branched Au nanostar¹³ structures. Among these nanostructures, the multi-branched Au nanostar features are especially attractive because of the crystallographically well-defined multiple Au branches with sharp tips that exhibit non-ordinary plasmon resonances, such as dipole and quadrupole resonances, which are not frequently observed in ensemble systems of unidirectional Au structures.^{13,14} Since Au nanoparticles have highly symmetric crystalline lattices, the formation of multi-branched structures requires organic stabilizing molecules for both prohibiting agglomeration and selectively passivating growth in certain planar directions. For example, organic stabilizing surfactants, including cetyltrimethylammonium bromide (CTAB), bis-(*p*-sulfonatophenyl) phenylphosphine dihydrate dipotassium, and sodium dodecyl sulfate (SDS), have been successfully used in synthesizing Au mono-, di-, tri- and tetrapod structures.^{11,15,16}

In many cases, seed Au nanoparticles have also been used to accelerate the growth of such multi-branched Au structures.¹⁷ Although the use of organic stabilizers is quite beneficial in preventing the severe aggregation of nucleated crystals and for efficiently guiding multi-branches, the presence of high molecular weight organic molecules serves as an electrical and photonic barrier, which eventually limits the mobility of charge carriers and excitons. Moreover, the transport of charge carriers in conducting metal particles is highly dependent on the shape and size of the particles at the nanoscale. Recently, Grzybowski and coworkers reported on the normal and inverse photoconductance behaviors of various alkyl thiol-capped gold and silver spherical nanoparticle thin films, in which the thiols were either charged or uncharged.⁹

Here, we report the growth of multi-branched gold star crystals on germanium (Ge) substrates using a surfactant-free spontaneous charge transfer reaction at room temperature. Unlike the conventional galvanic displacement process that uses a single solvent system, geometrically well-defined, multi-branched Au star structures have been obtained with a dimethylformamide (DMF)–water mixed solvent system. Interestingly, the photocurrent of the multi-branched Au stars was decreased by 10% when irradiated by a visible light laser. The detailed mechanism for the inverse photocurrent will be discussed.

Experimental section

Materials

Hydrogen tetrachloroaurate (HAuCl₄, 99.9+%) was purchased from Sigma Aldrich. All other chemicals, unless specified, were of reagent grade. Deionized water ($R > 18.0 \text{ M}\Omega$) was used to prepare the precursor solutions. A (100) Ge wafer (Ga-doped *p*-type (0.005–0.1 $\Omega \cdot \text{cm}$)) was used as the substrate.

^aDepartment of Materials Science and Engineering, Yonsei University, Seoul, 120-749, Korea. E-mail: wooyoung@yonsei.ac.kr; Fax: +82 2 312 5375; Tel: +82 2 2123 2834

^bDepartment of Chemistry, Korea University, Seoul, 136-701, Korea

^cDepartment of Nano-Physics, Gachon University, 1342 Seongnamdaero, Seongnam-si, Gyeonggi-do, 461-701, Korea

^dDepartment of Chemistry, Pohang University of Science and Technology (POSTECH), San 31, Hyoja-Dong, Nam-Gu, Pohang, 790-784, Korea

† Electronic supplementary information (ESI) available. See DOI: 10.1039/c3ta11983a

Gold star preparation

To synthesize multi-branched gold stars, 100 μL of a HAuCl_4 (10 mM) aqueous solution was added into 900 μL of dimethylformamide (DMF), generating a final 1.0 mM solution. A cleaned Ge substrate (5 mm \times 5 mm) was immersed into this solution. After 12 h, the Ge substrates with multibranched gold stars on their surfaces were thoroughly rinsed with deionized water to remove unreacted precursors and were then dried under ambient conditions.

Characterization

The transmission electron microscopy (TEM) and high-resolution TEM (HRTEM) images were obtained using a JEOL JEM-2100F (200 kV) transmission electron microscope equipped with a field emission gun and an ultrahigh-resolution observation system. The scanning electron micrographs were taken with a field emission scanning electron microscope (FESEM, JEOL Model JSM-7401F and FESEM, Phillips Model XL30S FEG). X-ray diffraction (XRD) patterns were obtained using a Bruker AXS D8 DISCOVER diffractometer with $\text{Cu K}\alpha$ (1.5406 \AA) radiation. X-ray photoelectron spectroscopy (XPS) measurements were performed using a VG Scientific ESCALAB 220 iXL spectrometer with a mono-chromated $\text{Al K}\alpha$ X-ray (1486.6 eV) as a light source. The base pressure of the chamber was 2×10^{-9} torr and the photoelectron take-off angle was 90° . The morphology changes of the multi-branched gold star crystals formed on the Ge substrates were investigated at the early stages using an atomic force microscope (AFM, Digital Instruments, Nanoscope IIIa, tapping mode).

Photocurrent measurement

Current was measured using a semiconductor analyzer (KEITHLEY 4200), and a solid-state laser (532 nm, 20 mV) was used as the light source.

Results and discussion

The spontaneous charge transfer-mediated formation of Au nanoparticles on a Ge substrate was first reported by the Buriak group.^{18–23} This reaction is also termed the galvanic displacement (GD) process because the charge transfer from Ge to Au ions is spontaneously induced by the intrinsic electrochemical potential difference, leading to the oxidation of Ge^0 and the reduction of Au^{3+} ions. Most of the metal nanostructures formed by the GD process have spherical shapes with varying sizes, regardless of the type of metal precursor and substrate. When a piece of Ge wafer was immersed in a HAuCl_4 (1 mM) aqueous solution for 12 h, a thin film of Au particles was spontaneously formed *via* the GD process (Fig. 1a). These results agree well with the previously reported spontaneous reduction of aqueous AuCl_4^- ions by Ge, which initiates the formation of spherical Au nanoparticles. In addition to the Au–Ge pair, numerous nano- and microparticles are spontaneously synthesized on various metals and semiconductor substrates, as long as their galvanic potential differences are thermodynamically favorable. Despite the advantages of the GD

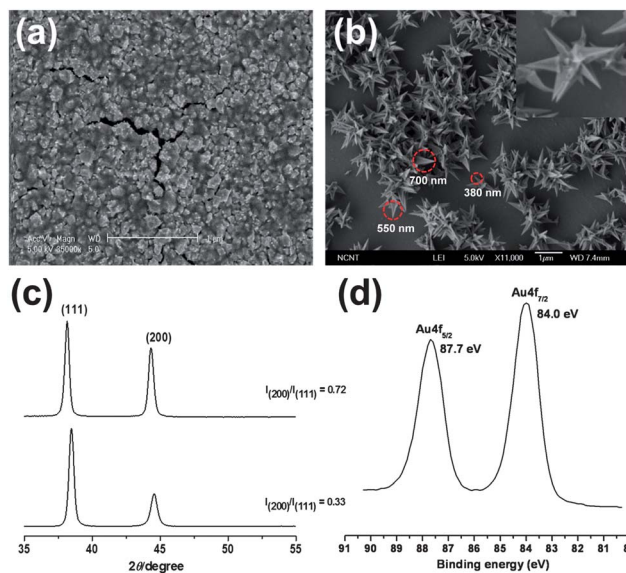


Fig. 1 SEM images of a gold nanoparticle film spontaneously deposited in 12 h on a Ge (100) surface from a 1 mM aqueous HAuCl_4 solution (a). Multi-branched gold stars spontaneously deposited in 12 h on a Ge (100) surface from a 1 mM DMF–water (9/1) mixed solvent system (b). XRD patterns of the fabricated gold film in pure water (lower trace) and the multi-branched gold star film in DMF–water (9/1, upper trace) (c). High-resolution Au 4f XPS features obtained from the multi-branched gold stars (d).

process in terms of simplicity and organic-free products, a serious disadvantage, the lack of shape selectivity, has blocked its high popularity.

In contrast to the conventional GD process, multi-branched Au star crystals were selectively formed *via* immersing the Ge wafer in a DMF–water (9/1 volume ratio) mixed solution with HAuCl_4 for 12 h (Fig. 1b). The sample consists of a large quantity of monodispersed multi-branched gold star particles. Each particle has numerous branches, and no other shapes were observed. The obtained multi-branched gold stars exhibit sub-micrometer sizes from one branch edge to another on the opposite side. The sizes of the branches in general follow Gaussian distribution and the average size was estimated to be 561 nm (Fig. S1†). Three representative branches, which correspond to the lower bound, a median, and the upper bound of the size distribution, are marked in Fig. 1b. Multiple branches were observed on each crystal, and each branch contains very sharp and clean facets similar to concave trigonal pyramidal facets (the inset in Fig. 1b). The basic crystal structure of multi-branched Au star crystals is identical to that of the Au film prepared from mono-solvent precursors. As shown in Fig. 1c, both the multi-branched Au stars (top trace) and Au particles (bottom trace) exhibit (111) and (200) major X-ray diffraction (XRD) pattern peaks in the 2θ range of $35\text{--}55^\circ$ that correspond to the (111) and (200) reflections of *fcc* metallic gold (JCPDS, 04-0784).

These results imply that the multi-branched Au star crystals are composed of pure crystalline gold. The XRD peak intensity ratio (0.72) of (200) to (111) diffractions ($I_{(200)}/I_{(111)}$) for the multi-branched particles is larger than that observed for the Au

particles (0.33). The value for the Au particle film agrees well with the conventional bulk intensity ratio (0.33).²⁴ Although these values represent the {111} planes that are the main crystal planes for both the Au star and the Au particle films, the high intensity ratio of the Au stars indicates that the growth rate of the gold star {100} planes is higher than that of the gold particle {100} planes. This growth rate difference is inferred to arise from the surface-selective stabilizing effect of DMF in competition with H₂O.

X-ray photoelectron spectroscopy (XPS) measurements confirmed the synthesis of multi-branched gold stars, which were completely reduced from AuCl₄⁻ ions into Au⁰. The high-resolution Au 4f XPS spectrum in Fig. 1d shows two distinctive metallic Au⁰ peaks at 87.7 eV and 84.0 eV, corresponding to 4f_{5/2} and 4f_{7/2} binding energies of metallic Au⁰, respectively.²⁵ No other features associated with Au⁺ and Au³⁺ were observed, which indicates that the AuCl₄⁻ ions were fully reduced by the GD process.

The effect of DMF was confirmed by an additional experiment, where gradually increasing amounts of DMF (10, 30, 60 and 90%) were added into the pure aqueous HAuCl₄ solution, and the growth of Au particles in the respective solution was observed. From this experiment, the Au branch structures begin to grow only above a certain DMF concentration ($\geq 60\%$) (Fig. 2). Based on this speculation, more DMF molecules are likely to be absorbed on the {111} planes and stabilize those planes, compared with the {100} planes, as the DMF concentration increases. In this situation, the Au stars gradually develop due to the reduction of Au cations in the solution onto the exposed Au crystal surfaces, mediated by the continuous supply of electrons from Ge. Additionally, the {100} planes have a relatively higher probability to be exposed for reaction with the precursor at higher DMF concentrations. However, the detailed mechanism for the Au star growth remains to be elucidated. The yield of multi-branched Au star crystals is directly proportional to their growth time. As shown in Fig. 3, the size and number of the branches become larger in proportion to the

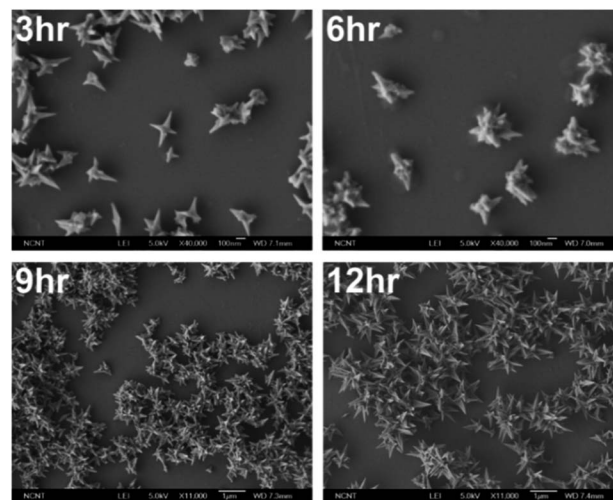


Fig. 3 The time-dependent shape development of gold stars after 3, 6, 9, and 12 h. The scale bars represent 100 nm (3 h, 6 h) and 1 μm (9 h, 12 h).

reaction time (3, 6, 9, and 12 h). Moreover, the sharpness and concaveness of the branches were also improved by prolonging the reaction time. Notably, no geometrically meaningful structures other than star crystals were observed on the Ge surface, which signifies the high selectivity of the GD process in the DMF–water mixed solvent system.

A further detailed structure of the multi-branched Au star crystals was investigated using high-resolution transmission electron microscopy (HRTEM) and selected-area electron diffraction (SAED) analyses. As shown in Fig. 4a and c, the tip of the Au branch has an apex diameter of approximately 10 nm, with a high crystallinity that is represented by clear lattice fringes. The lattice spacing is 2.37 Å, which is compatible with the (111) planes of *fcc* Au (2.36 Å, JCPDS, 04-0784). The SAED pattern taken from a branch of the Au star crystal shows an electron diffraction pattern that completely matches the *fcc* structure (Fig. 4b).

To understand the formation of multi-branches from the Au star crystals, atomic force microscopy (AFM) was utilized to investigate the morphology changes at the early growth stages. Fig. 5 shows the morphology changes of reduced Au on the Ge substrates after 10 s to 60 min. During the first 5 min, Au nanoparticles with a spherical shape are formed through homogeneous nucleation, similar to the previous report,¹⁸ and aggregated structures begin to form after 10 min. The branches

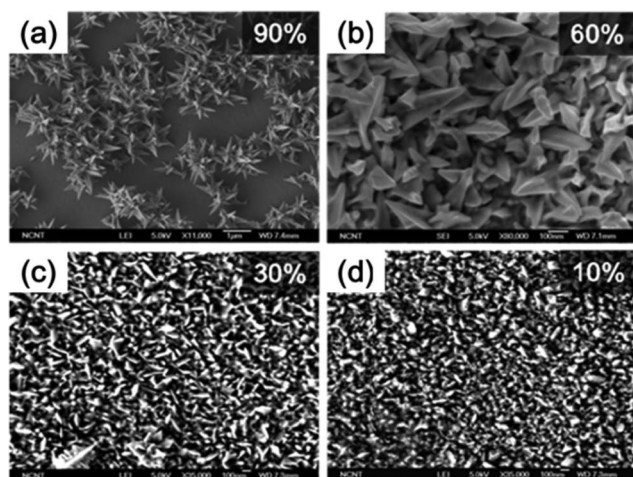


Fig. 2 SEM images of DMF volume-dependent gold structures: 90% (a), 60% (b), 30% (c), and 10% (d).

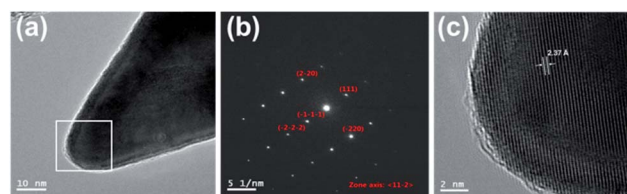


Fig. 4 (a) A TEM image of a branch, (b) the selected-area electron diffraction (SAED) pattern of (a), and (c) a magnified view of the HRTEM image of the squared region in (a). A *d*-spacing between adjacent lattice planes of 2.37 Å was found.

begin to form after 20 min and clearly develop 60 min after the reaction starts. The direct formation mechanism of the selective multi-branched Au star crystals *via* the GD process in a mixed solvent system is not clearly understood; however, DMF was found to play a critical role. Only spherical Au particles were formed in a pure water solvent system. Furthermore, no Au star crystals were obtained from other mixed solvent systems, such as 9/1 mixtures of dimethyl sulfoxide (DMSO)–water and pyridine–water (see Fig. S2†).

One possibility is the direct involvement of DMF in the reduction of AuCl_4^- ions. DMF is known to act as a reducing agent for Ag ions at room temperature.^{26,27} However, this possibility has been excluded in this research because it was confirmed by UV-vis spectroscopy that the DMF–water (9/1) mixed solution did not reduce the AuCl_4^- ions into Au^0 . The UV-vis spectra of HAuCl_4 displayed identical absorption peaks for both an as-prepared sample and a sample after 12 h in solution (Fig. 6). Another possible role of DMF is to hinder the crystal growth along a specific facet by selective adsorption on that facet while facilitating growth along other axes. The XRD data and the DMF concentration-dependent morphology changes support this assumption.

The photocurrent of the multi-branched gold stars was measured *via* visible laser irradiation at a constant time interval. The current decreased by 10% at a constant bias voltage of 0.001 V when the gold stars film was irradiated with a 532 nm laser (Fig. 7). The photoconductance of metal nanoparticles^{8,9} has been reported to show a normal positive photoconductance of gold nanoparticles capped with uncharged ligands, such as neutral alkyl thiols and alcohols. In these nanoparticles capped with uncharged ligands, Grzybowski

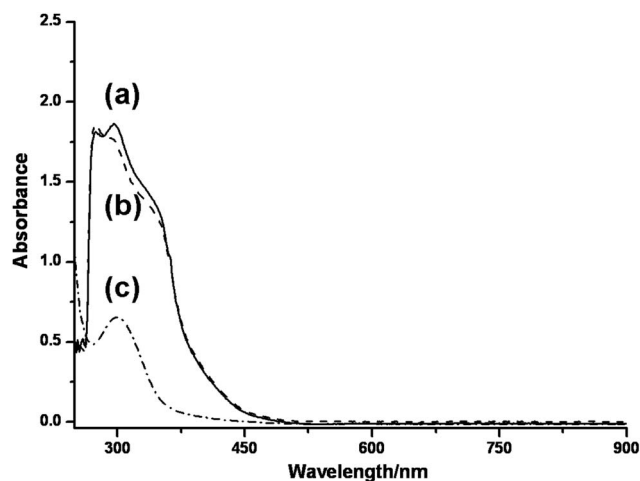


Fig. 6 UV-vis spectra of HAuCl_4 in DMF–water (9/1) after 12 h (a, solid), before 12 h (b, dashed), and HAuCl_4 in pure deionized water (c, dash dotted).

*et al.*⁹ reported that electrons move between neighboring nanoparticles by tunneling through a large barrier imposed by the insulating organic self-assembled monolayer (SAM). Upon illumination, the photoexcited plasmon resonance of the nanoparticles can promote electrons from the valence band to the conduction band of the nanoparticles, resulting in an increase in conductance.

Unlike their work,⁹ our photoelectric results exhibited an atypical inverse photocurrent in the multi-branched gold stars, in spite of using uncharged DMF ligand molecules. Additionally, it has been reported to show similar inverse photoconductance in charged thiol-capped metal particles.⁹ The

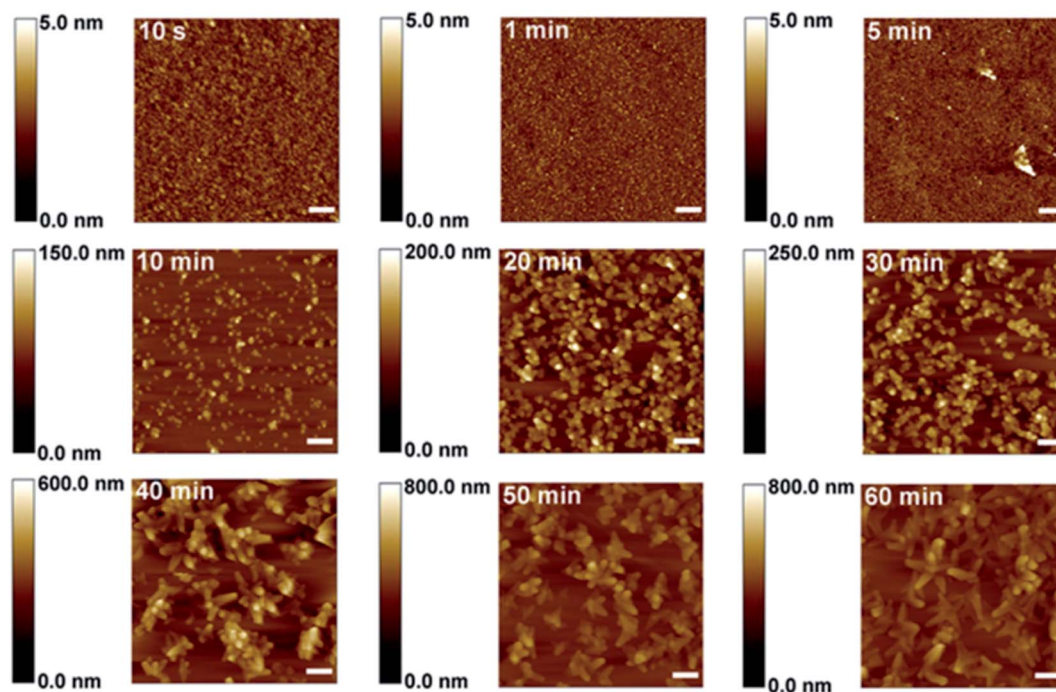


Fig. 5 AFM images of Ge (100) immersed into 1.0 mM HAuCl_4 in DMF–water (9/1) for various immersion times ranging from 10 s to 60 min. The grain sizes and deposition rates are tailored through carefully controlling the immersion time and reaction temperature. The scale bars represent 250 nm.

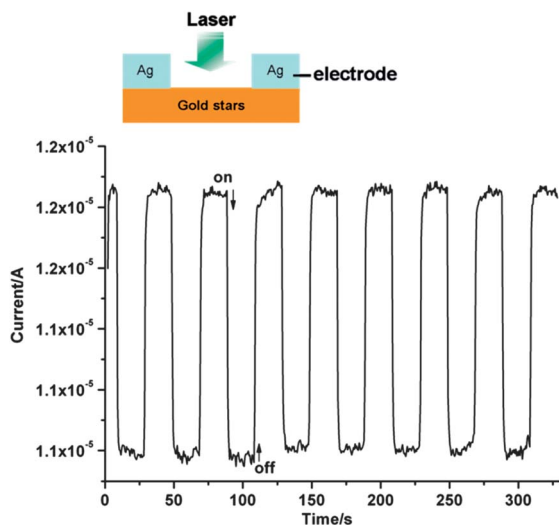


Fig. 7 The inverse photoresponse of a multi-branched gold star thin film.

inverse photoconductance occurred because the Fermi electrons that are excited from the valence band of the metal particles, due to illumination, are captured in low-lying polaron-like states stemming from the conformational rearrangement of the organic thiol molecules.⁹

In this study, the inverse photoresponse observed in the Au star structures is unique, although we used uncharged ligands in fabricating the nanostructures. The inverse photocurrent is related to the density and energy of the electron states, originating from the unusual Au star branch structures. As mentioned before, the branch tips are free from DMF, while the side facets of the branches are coated with neutral DMF. Consequently, electron transport is likely to occur due to electron tunneling through a thin barrier between adjacent branch tips. The electron density of states can be quantized near the tapered branch tips because the diameter of the branch tip is only ~ 10 nm, resulting in higher conduction states in the energy level. Contrastingly, the large surface area at the tips is favored to generate a high density of surface states between the valence and conduction bands. In this case, the photoexcited electrons 'fill' the available trap sites present on the nanoparticles, leading to a positive photocurrent.⁹ However, in the present work, the energy of photoexcited electrons can be higher than the lowest unoccupied molecular orbital (LUMO) level of the DMF ligands. In this case, the tunneling of electrons between the nanostar tips can occur in a negatively activated manner, leading to a decrease in conductance, *i.e.*, inverse photoconductance.

The photoresponse time was estimated to be 0.59 s at the same potential (0.001 V, see Fig. S3[†]). To understand the turn-on/off behavior, the irradiation was switched on and off >10 times. The same photoresponse repeatedly appeared without significant degradation, indicating the high reproducibility and reliability of the photoresponse (see Fig. 7). The photocurrent turn-on/off behavior by the incident light source of the same wavelength (532 nm) at 0.01 and 0.1 V (data not shown) was also observed.

Conclusions

Multi-branched gold stars were synthesized on semiconductor (Ge) substrates in high yield *via* a galvanic displacement method using a DMF–water (9/1) mixed solvent system at room temperature. The shape and sharpness of the multi-branched gold stars can be controlled through varying the reaction time and DMF volume fraction. A high volume ratio (90%) of DMF was found to be crucial for the formation of the multi-branched gold stars. A reasonable growth mechanism could be suggested through XRD and AFM studies. When irradiated with a visible laser (532 nm), the inverse photocurrent of the gold stars was demonstrated from systematic photocurrent measurements. The photocurrent of the gold stars decreased by 10% under illumination at 0.001 V. To investigate the turn-on/off response behavior, the irradiation was switched on and off >10 times, and the same photocurrent was repeated without significant degradation, demonstrating high reproducibility and reliability of the inverse photoresponse. The shape-controllable multi-branched gold stars can be used for applications that include high-efficiency photocurrent generation, photo-detection, light harvesting in photovoltaic cells, and supersensitive sensors.

Acknowledgements

This work was supported by the Priority Research Centers Program (2009-0093823) and the Converging Research Center Program (2012K001321) of the National Research Foundation of Korea (NRF). H. C. Choi is grateful for the financial support of a grant of NRF (2009-0094063).

Notes and references

- 1 C. Burda, X. Chen, R. Narayanan and M. A. El-Sayed, *Chem. Rev.*, 2005, **105**, 1025–1102.
- 2 N. L. Rosi and C. A. Mirkin, *Chem. Rev.*, 2005, **105**, 1547–1562.
- 3 G. A. Ozin and A. C. Arsenault, *Nanochemistry: A Chemical Approach to Nanomaterials*, RSC Publishing, Cambridge, 2005.
- 4 J. Cheon and J. -H. Lee, *Acc. Chem. Res.*, 2008, **41**, 1630–1640.
- 5 S. Dhar, E. M. Reddy, A. Shiras, V. Pokharkar and B. L. V. Prasad, *Chem.–Eur. J.*, 2008, **14**, 10244–10250.
- 6 H. Liu, D. Chen, F. Tang, G. Du, L. Li, X. Meng, W. Liang, Y. Zhang, X. Teng and Y. Li, *Nanotechnology*, 2008, **19**, 455101.
- 7 T. S. Hauck, T. L. Jennings, T. Yatsenko, J. C. Kumaradsa and W. C. W. Chan, *Adv. Mater.*, 2008, **20**, 3832–3838.
- 8 X. N. Xie, Y. Xie, X. Gao, C. H. Sow and A. T. S. Wee, *Adv. Mater.*, 2009, **21**, 3016–3021.
- 9 H. Nakanishi, K. J. M. Bishop, B. Kowalczyk, A. Nitzan, E. A. Weiss, K. V. Tretiakov, M. M. Apodaca, R. Klajn, J. F. Stoddart and B. A. Grzybowski, *Nature*, 2009, **460**, 371–375.
- 10 B. D. Busbee, S. O. Obare and C. J. Murphy, *Adv. Mater.*, 2003, **15**, 414–416.
- 11 S. H. Chen, Z. L. Wang, J. Ballato, S. H. Foulger and D. L. Carroll, *J. Am. Chem. Soc.*, 2003, **125**, 16186–16187.

- 12 K. Kwon, K. Y. Lee, M. Kim, Y. W. Lee, J. Heo, S. J. Ahn and S. W. Han, *J. Phys. Chem. C*, 2007, **111**, 1161–1165.
- 13 F. Hao, C. L. Nehl, J. H. Hafner and P. Nordlander, *Nano Lett.*, 2007, **7**, 729–732.
- 14 C. L. Nehl and J. H. Hafner, *J. Mater. Chem.*, 2008, **18**, 2415–2419.
- 15 E. Hao, R. C. Bailey, G. C. Schatz, J. T. Hupp and S. Y. Li, *Nano Lett.*, 2004, **4**, 327–330.
- 16 C.-H. Kuo and M. H. Huang, *Langmuir*, 2005, **21**, 2012–2016.
- 17 T. K. Sau and C. J. Murphy, *J. Am. Chem. Soc.*, 2004, **126**, 8648–8649.
- 18 L. A. Porter, H. C. Choi and J. M. Buriak, *Nano Lett.*, 2002, **2**, 1067–1071.
- 19 L. A. Porter, A. E. Ribbe and J. M. Buriak, *Nano Lett.*, 2003, **3**, 1043–1047.
- 20 M. Aizawa, A. Cooper, M. Malac and J. M. Buriak, *Nano Lett.*, 2005, **5**, 815–819.
- 21 M. Aizawa and J. M. Buriak, *J. Am. Chem. Soc.*, 2005, **127**, 8932–8933.
- 22 M. R. Nezhad, M. Aizawa, L. A. Porter, A. E. Ribbe and J. M. Buriak, *Small*, 2005, **1**, 1076–1081.
- 23 S. Y. Sayed, B. Daly and J. M. Buriak, *J. Phys. Chem. C*, 2008, **112**, 12291–12298.
- 24 X. Sun, S. Dong and E. Wang, *Angew. Chem., Int. Ed.*, 2004, **43**, 6360–6363.
- 25 K. Y. Lee, M. Kim, J. Hahn, J. S. Suh, I. Lee, K. Kim and S. W. Han, *Langmuir*, 2006, **22**, 1817–1821.
- 26 I. Pastoriza-Santos and L. M. Liz-Marzán, *Langmuir*, 1999, **15**, 949–951.
- 27 I. Pastoriza-Santos and L. M. Liz-Marzán, *Adv. Funct. Mater.*, 2009, **19**, 679–688.